Theor Chem Acc (2012) 131:1264
DOI 10.1007/s00214-012-1264-1

REGULAR ARTICLE

Metal-to-metal charge-transfer transitions: reliable excitation energies from ab initio calculations

Alex Domingo · Maria Àngels Carvajal · Coen de Graaf · Kanthen Sivalingam · Frank Neese · Celestino Angeli

Received: 16 May 2012 / Accepted: 23 July 2012 / Published online: 19 August 2012

Abstract A computational strategy is presented to describe excited states, involving the transfer of an electron from one metallic site to a neighboring metal center, the so-called metal-to-metal charge-transfer (MMCT) states. An accurate ab initio treatment of these states in transition metal compounds is intrinsically difficult for both time-dependent density functional and wave function-based methods. The rather large dependence of the MMCT energies on the applied functional makes difficult to extract reliable estimates from density functional theory, while the standard multiconfigurational approach (complete active space SCF + second-order perturbation theory) leads to severe intruder state problems and unrealistic, negative energies. The analysis of the failure of the multiconfigurational approach shows that the state-average orbitals are biased toward the ground state and strongly deficient to describe the MMCT state. We propose a method to improve the orbitals by gradually approaching as much as possible the state-specific description of the MMCT state in the reference wave function for the second-order perturbation treatment of the dynamic electron correlation.

Keywords Metal-to-metal charge transfer · Photomagnetism · CASPT2 · NEVPT2 · TD-DFT

Electronic supplementary material The online version of this article (doi:10.1007/s00214-012-1264-1) contains supplementary material, which is available to authorized users.

Dedicated to Prof. Ria Broer on the occasion of her 60th birthday.

A. Domingo · M. À. Carvajal · C. de Graaf (✉)
Departament de Química Física i Inorgànica, Universitat Rovira i Virgili, Marcel·lí Domingo s/n, 43007 Tarragona, Spain
e-mail: coen.degraaf@urv.cat

A. Domingo
Laboratoire de Chimie Quantique, Institut de Chimie UMR 7177, Université de Strasbourg, 4 rue Blaise Pascal, 67000 Strasbourg, France

C. de Graaf
Institució Catalana de Recerca i Estudis Avançats (ICREA), Passeig Lluís Companys 23, 08010 Barcelona, Spain

K. Sivalingam · F. Neese
Max-Planck-Institut für bioanorganische Chemie, Stiftsstraße 34-36, 45470 Mülheim an der Ruhr, Germany

C. Angeli
Dipartimento di Chimica, Università di Ferrara, via Borsari 46, 44121 Ferrara, Italy

1 Introduction

The self-consistent field calculation with exchange of Hartree in 1936 for the Cu^+ ion can be considered as the first Hartree–Fock treatment of a transition metal [1]. An important advance was made when the largely manual approach could be replaced by a procedure using electronic computers in the late 1950s. One of the first examples is the calculation of the radial Hartree–Fock wave functions for V^{2+} by Beatrice Worsley in 1958 [2] using the Numerov numerical integration scheme. Simultaneously, Watson performed Hartree–Fock calculations following the procedure outlined by Roothaan [3] with a Slater type orbital (STO) basis set on the complete series of first row transition metals [4]. Henceforth, the foundations for ab initio calculations on molecular complexes were laid by Richardson and co-workers who developed a smaller STO basis set for the transition metals [5]. Three years later Nieuwpoort published a monograph [6] on the non-empirical treatment of the electronic structure of $Ni(CO)_4$, $[Co(CO)_4]^-$ and $[Fe(CO)_4]^-$ using the previously developed basis sets.

After this pioneering work [7, 8], calculations on the hexafluoro complexes of Ti, Cr, Fe, and Ni were performed [9] and an interesting step forward was made by Gladney and Veillard who introduced the Gaussian type orbitals in the treatment of transition metal complexes [10]. A very early calculation on a binuclear complex—a molecule or cluster that contains two transition metal ions—was performed by Wachters and Nieuwpoort who calculated the coupling between the spin angular momenta of two Ni^{2+} ions in $KNiF_3$ [11, 12].

The efforts of quantum chemists have not ceased ever since to obtain more and more accurate descriptions of the electronic structure of transition metal compounds. In the first place, the development of efficient computational schemes to include electron correlation has had (and still has) a major impact in the field for the obvious reason that the mean-field treatment of the electron–electron interaction introduces serious artifacts when transition metals are present in the system. Secondly, the increase in computational power made possible to tackle systems with one or more transition metals and rather bulky ligands with sophisticated schemes; an accurate ab initio treatment of transition metal complexes with up to 200 atoms is certainly within reach nowadays.

Among the many properties of transition metal complexes, the possibility to change the magnetic properties of some compounds by shining light on them is especially interesting for its potential application in the development of new materials with bistable properties. In this aspect, it is highly desirable that the sample can be switched back and forth on a short time scale and preferably at room temperature. Both conditions are not easily achieved, although important advances have been made recently [13].

One of the first well-documented examples of photomagnetism concerns the light-induced excited state spin trapping (LIESST) process in Fe^{II} complexes [14, 15]. In this case, the system is excited from its non-magnetic singlet ground state to higher-lying ligand-field or metal-to-ligand charge-transfer states. The excited state rapidly decays non-radiatively to the Fe^{II} high spin state via internal conversion and intersystem crossings [16–19]. The deactivation of the metastable high spin state is relatively slow and can take place on a nanosecond timescale [20] or last for several days [21]. Moreover, the LIESST effect has also been described in binuclear Fe^{II} complexes [22–24].

A different kind of light-induced magnetism is observed in the Prussian-blue analogs. In this case, the electronic excitation changes the formal oxidation states of two neighboring metals through a metal-to-metal charge-transfer (MMCT) process. A well-documented case is the $Fe^{II}Co^{III}$ system [25–28], for which the non-magnetic ground state can be switched to a magnetic state with light of $\sim$500–750 nm. The irradiation causes the transfer of one electron from Fe to Co, changing the ground state closed shell $3d^6$ configuration of the two ions to open-shell Fe-$3d^5$–Co-$3d^7$ configurations. The resulting non-zero spin angular moments on the metals are coupled antiferromagnetically resulting in a ferrimagnetic behavior of the compound.

The same phenomenon has been observed in molecular complexes. One of the first examples was the octacyanomolybdate studied by Herrera et al. [29]. The increase in the magnetic susceptibility observed upon irradiating the sample at low temperatures was explained by a MMCT excitation from the central diamagnetic Mo^{IV}-$4d^2$ ion to one of the six peripheral Cu^{II} ions. In this way, a relatively strong coupling of the spin angular moments is enabled between the remaining five Cu^{II}-$3d^9$ ions and the central Mo^{IV}-$4d^1$ ion, which turns the magnetic behavior of the molecule from paramagnetic to ferromagnetic after irradiation. Recently, an alternative mechanism has been proposed for light-induced magnetism in cyanomolybdates. Circular dichroism experiments reveal the formation of a high spin $Mo^{IV}(S = 1)$ state upon irradiation [30] pointing to a spin crossover mechanism for the light-induced magnetism, which is in some sense similar to what is observed in the Fe^{II} compounds. The ab initio calculations by some of us [31, 32] point in the same direction. The excited $Mo^{IV}(S = 1)$ state is stabilized by a change in the coordination sphere from dodecahedral to square antiprismatic and subsequently the central Mo^{IV} ion looses one of its eight ligands ending up with a pentagonal bipyramid coordination sphere.

Metal-to-metal charge transfer does not only play a fundamental role in the light-induced magnetism [33, 34] but is also at the very basis of many other interesting phenomena, like photocatalytic activity and light-harvesting properties or photo induced electron transfer [35, 36]. Furthermore, important efforts have been made to design complexes in which the MMCT state is sufficiently long-lived to observe emission from it [37]. The process has also been invoked to explain the lowest peak in the optical absorption spectrum of $LaMnO_3$ [38], the parent compound of the manganites with colossal magnetoresistance. Finally, it is worth mentioning that the MMCT configurations play a central role in the phenomenological models to explain the coupling of localized spin angular momenta in (anti-)ferromagnetic systems [39–44].

The ab initio description of MMCT excited states or the metal-to-metal electron transfer process is obviously a non-trivial task. A density functional theory (DFT)-based approach may very well suffer from the well-known difficulties to describe charge-transfer states by means of the time-dependent variant of DFT (TD-DFT) [45–47]. Additionally, there seems to be no consensus yet on the optimal choice of functional for the treatment of excited states in TD-DFT for system containing transition metals, the

scattering of the obtained energies is rather large [48]. On the other hand, a wave function-based approach (post Hartree–Fock method) may become difficult due to the larger system size of the binuclear compounds and the inherent increase in computational requirements. Moreover, there is also an issue with the orbital optimization process in the latter approach, which has a large influence on the description of the MMCT states and that will be discussed in more detail on the next sections. In short, there is no well-established computational strategy to accurately describe MMCT states in transition metal complexes. This seriously hampers the progress toward a detailed understanding of many interesting phenomena.

The main purpose of the present work is to fill this lacuna, and we have developed a new approach to obtain a balanced description of ground and excited states with multiconfigurational perturbation theory. To this purpose, we will first review the problems that arise with a standard complete active space self-consistent field (CASSCF) wave function and investigate the behavior of TD-DFT in two model systems. The analysis of the failure of the CASSCF approach gives the keys to modify the strategy and obtain a reliable description of the MMCT states.

2 Standard approach

The first model system that we handle is based on the perovskite structure La_2NiO_4, in which Ni^{2+} ions are located in the center of corner sharing elongated octahedra of O^{2-} ions. An embedded cluster with two metal sites is constructed following the standard procedure [49–52]. The two metal sites and their first neighbors (eleven O^{2-} ions) define the all-electron cluster. This group of atoms is embedded in a set of point charges that reproduce the Madelung potential both in the cluster region and in a shell of pseudo potentials [53, 54] surrounding the cluster to separate the cluster electron density from the point charges. A simple yet relevant model to describe MMCT states was obtained by replacing one of the Ni^{2+} ions for a Cu^{2+} ion. In this way, there are only three unpaired electrons in the system, which facilitates the analysis of the possible problems in the CASSCF treatment.

The second model system is taken from our previous study of the copper octacyanomolybdates [31, 32] and consists of a binuclear system with a Cu^{II}–NC–Mo^{IV} central unit. The coordination sphere of the copper ion is completed with a tris(2-aminoethyl)amine (tren) ligand and Mo is saturated with two CN^- ligands and five CNH ligands, which mimic the CN–Cu(tren) ligands of the real molecule. This modeling was carefully checked in our previous studies of the molecule and has also been used by others in related complexes [55]. A graphical representation of the two model systems can be found in Figure 1 and will be referred to as CuNi and CuMo from now on.

The ground state of the CuNi cluster is a doublet state arising from the antiferromagnetic coupling of the local triplet state (two unpaired electrons) on the Ni^{2+}-$3d^8$ ion and the doublet state (one unpaired electron) of the Cu^{2+}-$3d^9$ ion. In principle two MMCT states can be considered in this cluster: from Ni → Cu or vice versa. We only consider the lowest one, which corresponds to the electron movement from Ni to Cu as a balance of the ionization potentials and electron affinities of the two metals. Hence, a complete active space (CAS) to expand the wave functions for ground and MMCT states should contain at least the three electrons and three orbitals shown in the left column of Figure 2. This CAS(3,3) defines, however, much more doublet coupled states. The left column of Figure 3 illustrates that the lowest excited roots are characterized by electron replacements within the two active orbitals centered on the Ni^{2+} ion, so-called *d–d* transitions. The MMCT state only appears as the fifth root in the CASSCF calculations, and hence, a state-average (SA) procedure with five roots is necessary in the standard approach (SA-CASSCF) commonly used to study electronically excited states in molecular systems [56–61].

A similar reasoning can be followed for the CuMo dimer. The ground state is formed by the Mo^{IV}-$4d^2$ –Cu^{II}-$3d^9$ electronic configuration, where the two Mo-*d* electrons are paired up in the lowest 4*d* orbital of approximate $4d(z^2)$ character. The MMCT state has a Mo^{V}-$4d^1$ –Cu^{I}-$3d^{10}$ configuration. Similarly to the CuNi case, this state is not the first excited state of the CAS(3,3) that is spanned by the active orbitals shown in the right column of Figure 2. In between, there are three Mo *d–d* transitions of lower energy.

As a first step, we perform a SA-CASSCF with these five roots, meaning that each state has a weight of 20 % in the orbital optimization process. From the schematic representation of the electronic configurations given in the right part of Figure 3, it can be seen that the second root ($\Delta E = 1.8$ eV) has a triplet coupled open-shell Mo-$4d^2$ configuration and that the third root is the equivalent state with local singlet coupling located at 2.6 eV. The fourth root arises from a double *d–d* transition on Mo and has significantly higher relative energy (6.5 eV) than the other two *d–d* transitions. Finally, the MMCT state is found at 12.5 eV.

Naturally, this CASSCF description of the electronic states is not the final answer. It almost completely lacks the effect of dynamic electron correlation and, therefore, should be followed by either a multiconfigurational reference (MR) configuration interaction as done in Refs. [62–65] or MR second-order perturbation theory (PT2), which is more

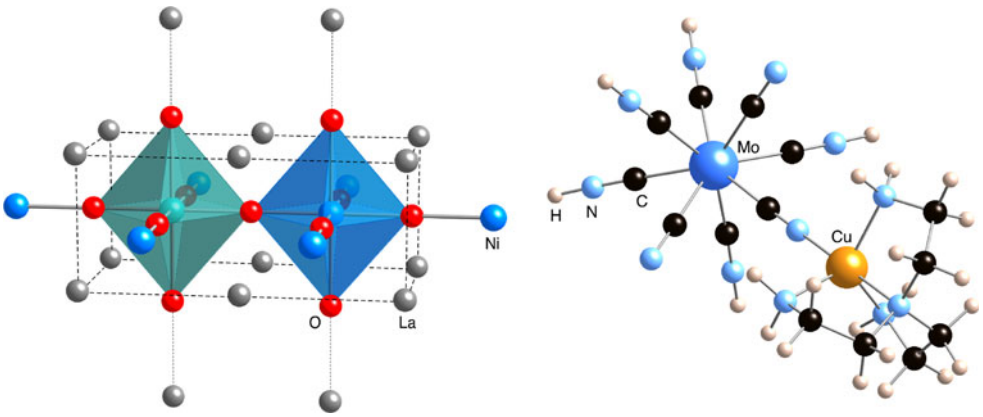

Fig. 1 The two model systems considered in the study of the MMCT states. On the *left*, an embedded $(Cu,Ni)O_{11}$ cluster (CuNi). The *blue* octahedron has a Cu^{2+} ion in the center and the *green* one contains a Ni^{2+} ion. The *dashed black lines* are a guide to the eyes. On the *right*, the Mo–CN–Cu dimer (CuMo) as a model for the copper octacyanomolybdate

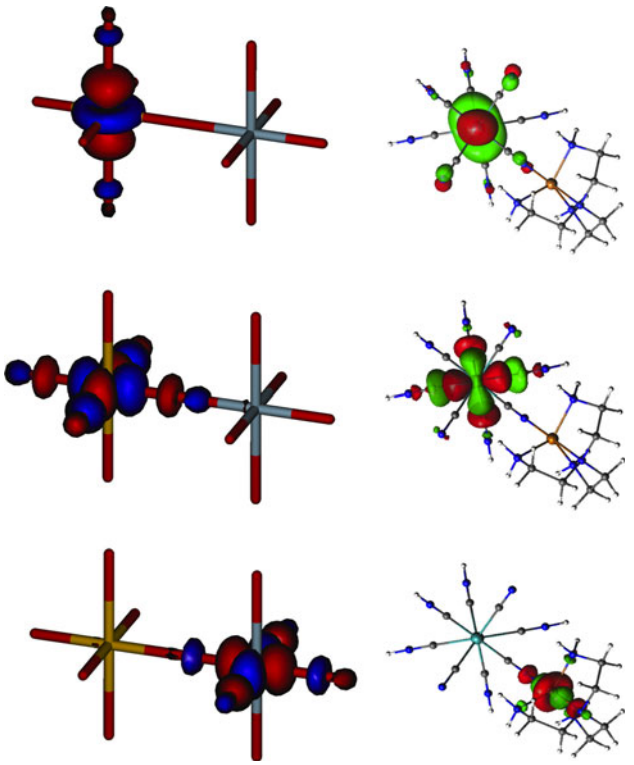

Fig. 2 Active orbitals of CuNi (*left*) and CuMo (*right*) obtained from a state-average CASSCF(3,3) calculation for the lowest five doublet states. The Cu atom is located on *right side* in both models

often applied. Among the different MR-PT2 implementations, the CASPT2 variant [66, 67] has been especially successful in the description of excited states in a large variety of organic and inorganic systems [68–73]. However, the description of the MMCT state in the present system is highly deficient. The solution of the CASPT2 equations does not converge in a reasonable number of iterations and erratic relative energies were obtained. The problem could not be solved with the (imaginary) level shift technique [74, 75] as shown in Table 1. The convergence problems persist up to values of 0.4 au. Although the calculation converges for larger shifts, the relative energy of the MMCT state with respect to the ground state (calculated with the same level shift) is by no means stable and no conclusive answer can be obtained. The problem is not exclusive for the CASPT2 method. We also tried the *n*-electron valence state implementation of MR-PT2 (NEVPT2) [76–78]. This variant is based on a zeroth-order Hamiltonian with explicit two-electron terms for the active orbitals and very rarely suffers from the intruder state problem. Nevertheless, the method also produces an unrealistic, negative excitation energy for the MMCT state.

It is well-known that MR-PT2 is not able to provide correct results when the reference wave function lacks important configurations. In the present case, we have investigated whether an extension of the active space with ligand-to-metal charge-transfer configurations improves the CASPT2 behavior. Unfortunately, it is not possible to restrict the extension of the active space to a few well-defined CN-π/π^* orbitals in the CuMo model. The orbital optimization process turns the new active orbitals in Cu-3*d* and 3*d*′ orbitals due to the second *d*-shell effect [61, 79]. Therefore, we optimized the wave function with an active space of 12 metal orbitals (2 Mo-4*d* + 5 Cu-3*d* + 5 Cu-3*d*′) and two CN orbitals ($\pi + \pi^*$) localized on the CN group that bridges Cu and Mo. In principle, this extension would certainly help to improve the description of the MMCT state, but the number of roots that span the active space has increased enormously and there appear many new roots with lower relative energy than the MMCT state. In fact, we have not been able to localize the MMCT state among the first twelve roots. These lower-lying roots are either due to local *d*–*d* transitions on Cu or Mo or arise from electron transfers between the CN ligand and the metals. Therefore, we conclude that, generally speaking, the extension of the active space is not the way to follow to improve the description of the MMCT state.

At difference from the above-described behavior for MMCT states, the standard approach based on SA-CASSCF reference wave functions can give accurate results for

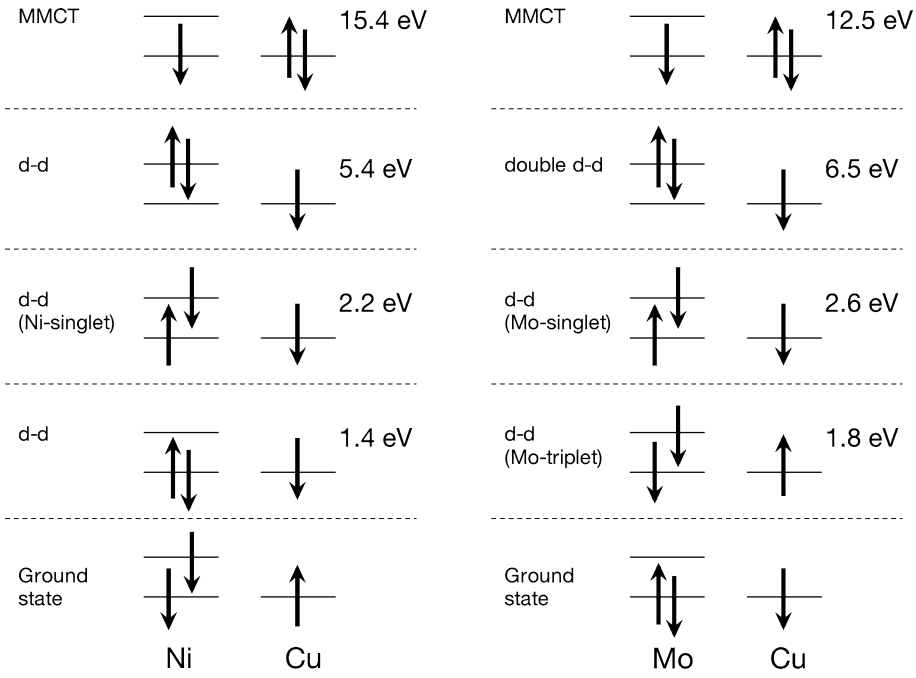

Fig. 3 Schematic representation of the electronic configurations of the five lowest doublets in CuNi (*left*) and CuMo (*right*). The energies refer to the SA-CASSCF results with equal weights for all states

Table 1 CASPT2 relative energies of the MMCT state in the CuMo dimer as function of the imaginary level shift

Level shift (au)	ΔE (eV)	Ref. weight
0.00	2.73	Not converged
0.10	1.97	Not converged
0.20	−18.21	Not converged
0.30	−17.81	Not converged
0.35	1.94	Not converged
0.40	3.07	0.363
0.45	3.60	0.375
0.50	3.99	0.384
0.60	4.62	0.401

The reference wave function is based on a state-average CASSCF wave function for the five lowest doublets with a minimal active space containing three orbitals and three electrons

relative energies in excitations involving only one TM. The SA-CASSCF procedure is not only successfully applied to calculate the relative energies of states with the same number of *d*-electrons but also to describe ligand-to-metal or metal-to-ligand charge-transfer states, and other cases in which the electronic configuration changes between the ground and excited state. A small (incomplete) sample of such calculations can be found in the Refs. [80–89]. There are of course exceptions to this general behavior, in which better agreement with experiment is obtained applying single-state optimization procedures [90–92], but these are either due to the large number of roots that need to be considered before including the state of interest in the averaging procedure or to the impossibility to provide enough flexibility to the wave function due to the limitation of the size of the CAS. This is exactly what happens for the MMCT states described above, although the problems are less severe when only one TM ion is involved.

3 Toward a single-state description

In the CuMo model, the four lowest states are all characterized by a Mo^{IV}–Cu^{II} electronic configuration, meaning that this electron distribution has a weight of 80 % in the orbital optimization procedure. The fifth root in the state-average CASSCF calculation—the MMCT state with a Mo^{V}–Cu^{I} configuration—only contributes 20 %. The low weight of the MMCT state in the orbital optimization procedure causes the resulting orbitals to be strongly biased toward the "*neutral*" electron distribution. It is worth noticing that the optimal metal orbitals for the "*neutral*" (GS and *d*-*d*) electron distributions are rather different from those of the "*ionic*" (MMCT) electron distribution as a consequence of the different occupation number of the metal *d* orbitals. For this reason, the orbital optimization procedure based on the SA-CASSCF strategy is forced to find a compromise between the conflicting requirements of the different states. This is nicely illustrated by the maximum elements of the orbital gradient values of the individual roots at convergence of the SA-CASSCF. The first four roots have all values close to 4.5×10^{-2}, whereas the MMCT state has a much bigger element of −0.18 The shortcomings in the orbitals cannot be repaired by the

approximate treatment by CASPT2 of the off-diagonal part of the Fock operator connecting the three orbital spaces (inactive-active-virtual). Furthermore, as shown in Sect. 2, the extension of the active space does not improve the description of the MMCT state. The increase in the number of states available with larger active spaces actually turns out to deteriorate the MMCT description.

Based on these observations, we made some modifications to the standard approach to describe excited states in transition metal complexes. In the first place, we decided to stick to a minimal active space to have the MMCT state as low as possible in the list of roots. The price to pay is that we do not include the double *d*-shell effect and introduce a small uncertainty in the excitation energies. In the second place, we leave aside the state-average procedure and try to obtain a description of the orbitals as close as possible to a hypothetical single-state description of the MMCT state. Note that in practically all cases, it is impossible to optimize the wave function of higher roots in a single-state calculation due to root flipping problems. Instead, we perform a series of calculations with increasing weight on the MMCT state in the orbital optimization procedure and carefully check the convergence of the results. In this way, we eliminate the arbitrariness of the results that could be introduced by differently weighting the roots in the CASSCF. Finally, we use a state-specific description for the ground state. All the reported excitation energies are calculated with respect to this state.

3.1 The CuNi model

The modified computational scheme was first tested in the CuNi model. Figure 4 shows how the CASSCF energies of the five roots evolve with increasing weight on the fifth root, the MMCT state. The energy of the first four roots gradually increases with respect to the single-state description of the ground state in a nearly parallel manner. On the other hand, the MMCT state is significantly lowered in energy from approximately 16 eV in the SA-CASSCF calculation with equal weights to 10 eV when the state has 63.6 % weight in the state average. At this point, the energy of the double *d*–*d* transition (root 4) nearly coincides with that of the MMCT state. A further increase in the weight leads to root flipping problems, and the orbital optimization procedure does not converge anymore. Hence, this is as close as we can get to a single-state description of the MMCT state, which is obviously relatively far to a real state-specific description of the MMCT state, but the curve suggests that further improvements on the orbitals would only lead to a modest lowering of the MMCT energy.

The next step is to include the dynamic electron correlation, which is expected to have a significant differential

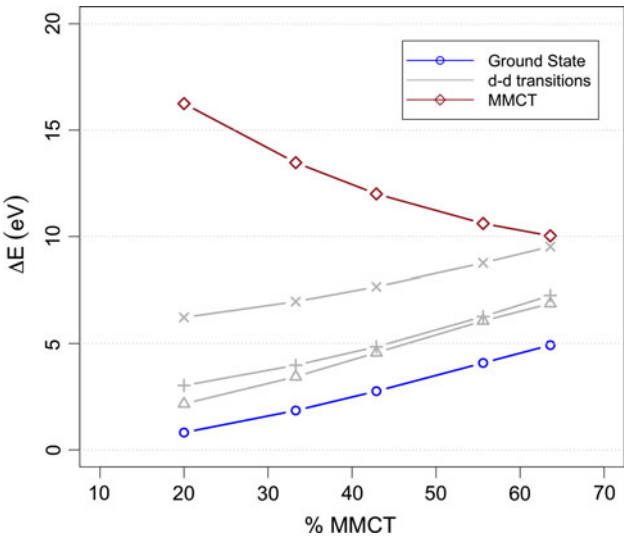

Fig. 4 State-average CASSCF energies (in eV) of the five lowest doublets of CuNi as function of the weight of the MMCT state in the orbital optimization. The state-specific CASSCF of the ground state is taken as reference energy

effect on the relative energy of the MMCT state given the changes in the number of *d*-electrons on the two metal ions. The CASPT2 calculation with the standard SA-CASSCF wave function as reference (i.e., with a 20 % weight of the MMCT state) behaves identically as for the CuMo model (Table 1). The calculation only converges for very large level shifts, and no plateau in the relative energy was observed for shifts below 0.7 au. The left panel of Figure 5 shows the unrealistic behavior of CASPT2 for this reference wave function. The situation is improved when the CASSCF wave function is optimized for an average of states in which the MMCT has a higher weight. The mid-panel shows that for 42.9 % MMCT weight, the CASPT2 is still deficient for small level shifts but above 0.25 au. starts to become more stable, although the relative energy cannot be considered to be independent of the shift applied. A completely different and much more satisfactory picture is obtained when the weight of the MMCT state in the orbitals optimization is still further increased to 63.6 %. The right panel shows that the relative CASPT2 energy of the MMCT states obtained with this reference wave function is nearly independent of the level shift and only suffers from a weak intruder state problem around 0.04 au. The curves for all five reference wave functions and the dependence of the weight of the CASSCF wave function in the corrected wave function as function of the level shift can be found in the supporting information.

Comparing the five reference wave functions, it is clear that the CASPT2 results gradually improve and reach convergence for the reference wave function with the highest weight on the MMCT state in the orbital

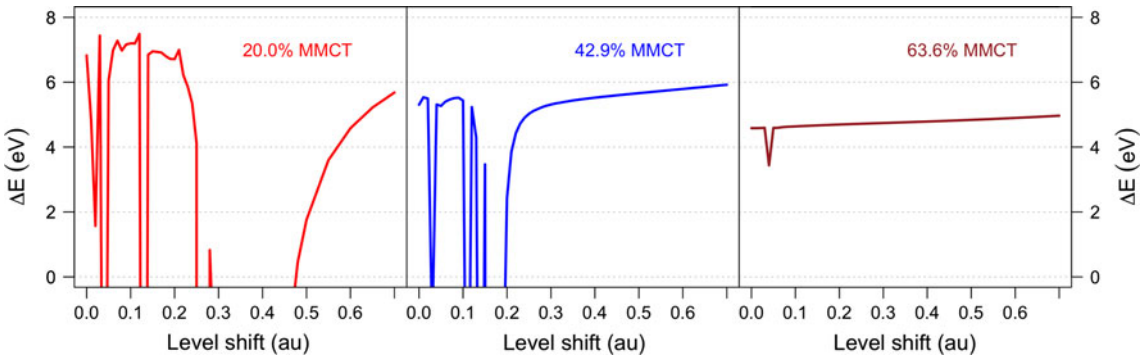

Fig. 5 CASPT2 vertical excitation energy (in eV) of the MMCT state of CuNi as function of the level shift. Three reference wave functions with different weights are compared

optimization. Our final estimate of the excitation energy is 4.6 eV, referring to the unshifted CASPT2 result based on the 63.6 % reference wave function. Note that the dynamic electron correlation has a major effect on the excitation energy of the MMCT state. Figure 4 shows that CASSCF predicts a value of slightly lower than 10 eV, while CASPT2 lowers this by about 5 eV.

3.2 The CuMo model

The same procedure has been followed to obtain a reliable estimate of the MMCT excitation energy for the CuMo model. Figure 6 shows the evolution of the CASSCF energies of the five lowest roots of the CAS(3, 3) (see Fig. 3, right column) as function of the weight of the MMCT state used in the orbital optimization procedure. The behavior is rather similar to the one observed for the CuNi model: the lowest states with the same electronic configuration are uniformly raised in energy, while the MMCT state is lowered.

The MMCT state becomes nearly degenerate with the fourth root (a double *d*–*d* transition) at slightly less than 50 % weight. Larger weights lead to root flipping, but by stopping the orbital optimization after the iteration where root flipping took place, we could continue the process with one root less (the double *d*–*d* transition) without loosing the MMCT state in the state average. This reduction of the number of roots makes it possible to get converged wave functions with larger weights on the MMCT state up to 62.5 %. The maximum element of the orbital gradient for the MMCT state is about 2.5 times smaller than in the initial standard SA-CASSCF wave function, indicating that the orbitals are better suited to describe the situation where one electron is transferred from Mo to Cu. When the weight is increased beyond 62.5 %, root flipping problems are encountered again. Unfortunately, it was not possible to repeat the strategy followed around 50 % to get rid of even more roots. Root flipping problems persist and no wave

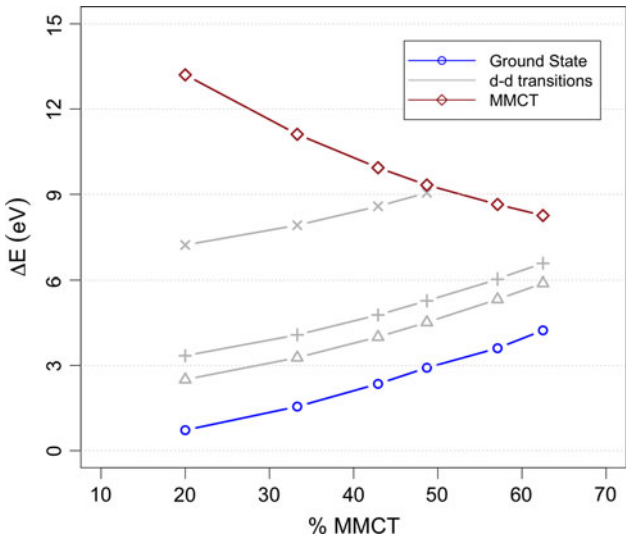

Fig. 6 State-average CASSCF energies (in eV) of the five lowest doublets of CuMo as function of the weight of the MMCT state in the orbital optimization. The state-specific CASSCF of the ground state is taken as reference energy

function could be converged with larger weight than 62.5 % on the fourth root without loosing the MMCT state. Again, the CASSCF energy of the MMCT state with respect to the single-state description of the ground state is not completely converged but not too large changes are expected.

The results of the CASPT2 calculations as a function of the imaginary level shift are summarized in Fig. 7. In line with the previous findings, we see that the CASSCF wave function with equal weights on all five roots (20 %) gives very poor results for the MMCT state. The situation gradually improves when the weight of the MMCT state is increased to 42.9 % (mid-panel), and we get excellent results for 62.5 %, shown on the right. The CASPT2 energy obtained with this reference wave functions is practically independent of the level shift. This is a strong indication that the orbitals are sufficiently well suited to

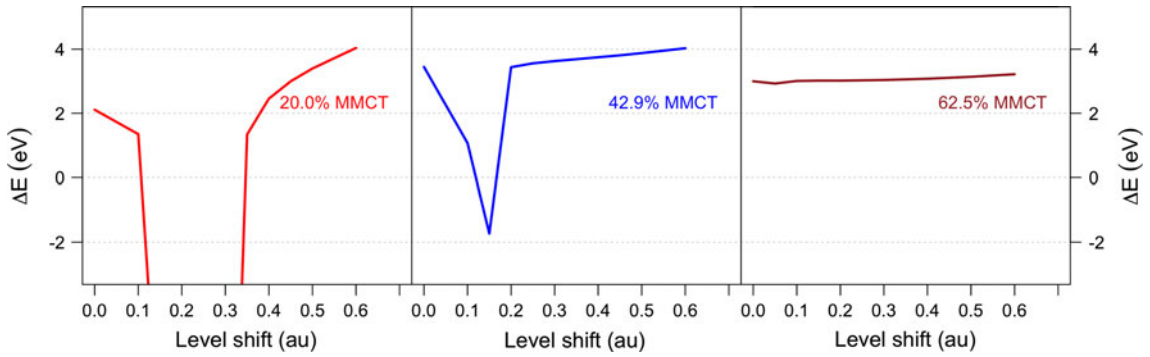

Fig. 7 CASPT2 energy (in eV) of the MMCT state of CuMo as function of the level shift. Three reference wave functions with different weights are compared

describe the MMCT state. The final estimate of the transition energy is 3.0 eV, extracted from the CASPT2 calculation with zero level shift and using a reference wave function with 62.5 % weight on the MMCT state in the orbital optimization process.

3.3 Wave function analysis

In the famous study of Fujimori and Minami of the ionic insulator NiO [93], it is stated that the intense optical absorption starting at $\approx$4.0 eV is not only due to oxygen-to-Ni excitations as was generally assumed at that time, but it has also important contributions from MMCT excitations. However, it was also recognized that the characterization of the excited states is far from trivial due to the large configuration mixing in their parametrized CI approach and that the distinction between MMCT and ligand-to-metal charge-transfer (LMCT) states is somewhat artificial in their calculations. Here, we deal not only with the configuration mixing but also with independent orbital optimizations for each state. To ensure that the root that we mark as MMCT state in CuMo is actually the result of an electron transfer from Mo to Cu, we have analyzed the wave function of ground and excited state by looking at (1) the natural orbitals and their occupation numbers; and (2) the overlap of the two *N*-electron wave functions involved in the MMCT excitation.

To start with the latter, in a standard SA-CASSCF approach, all the states are of course orthogonal and no special actions need to be taken. As soon as the *N*-electron wave functions are not expressed in a common orbital set, but have the same spatial and spin symmetry, orthogonality should be checked and eventually restored through non-orthogonal CI [94] or the state interaction (SI) procedure [95]. The first wave function in the SI treatment is the one that is obtained from the single-state CASSCF optimization of the ground state, Ψ_{GS}. The second wave function describes the fourth root in the SA-CASSCF with 62.5 % weight on the fourth root, that is, the wave function that maximally resembles the hypothetical single-state description of the MMCT state, Ψ_{MMCT}. The SI shows that both the overlap integral ($\langle\Psi_{GS}|\Psi_{MMCT}\rangle = -0.0027$) and the interaction matrix element ($\langle\Psi_{GS}|\hat{\mathcal{H}}|\Psi_{MMCT}\rangle = 18.5$ au) are very small. The total energies of the final states differ by less than 1 meV from the initial states, and therefore, the non-orthogonality effect can be neglected.

The three natural orbitals of Ψ_{GS} and Ψ_{MMCT} resemble the active orbitals shown in the left column of Fig. 2. The only obvious difference is that the natural orbitals of Ψ_{MMCT} are slightly more delocalized than the ones obtained in the standard SA-CASSCF calculation, especially the Cu-3*d* and the Mo-4$d(x^2 - y^2)$ orbitals (see Supp. Info.). The Ψ_{GS} natural occupation numbers are 1.9907, 0.0093, and 1.0000 for the Mo-4$d(z^2)$, Mo-4$d(x^2 - y^2)$, and Cu-3*d* orbitals, respectively. This changes to 1.0000, 0.0000, and 2.0000 for the Ψ_{MMCT} state, exactly coinciding with the transfer of one electron from a highly localized Mo-4*d* orbital to a slightly more delocalized Cu-3*d* orbital. Therefore, the energy difference between the states characterized by these natural orbitals can be considered as the MMCT transition energy.

3.4 NEVPT2 calculations

To rule out the possibility that the erratic outcomes of the CASPT2 calculations when reference wave functions are used with not too high weight on the MMCT is caused by the approximate nature of $\hat{\mathcal{H}}^{(0)}$, a series of calculations was performed with another MR-PT2 scheme, namely the aforementioned NEVPT2 approach. Table 2 resumes the results of the NEVPT2 calculations for the CuNi cluster model with the same reference wave function as used in the CASPT2 calculations. The results of the strongly contracted variant (sc-NEVPT2) are practically the same as for the partially contracted version (pc-NEVPT2), despite the much smaller number of perturber functions in the former. Such behavior has been observed more often [96, 97] and

Table 2 Strongly contracted and partially contracted NEVPT2 relative energies (in eV) of the MMCT state in the CuNi dimer as function of weight of the MMCT state in the SA-CASSCF reference wave function

% MMCT	sc-NEVPT2	pc-NEVPT2
20.0	−3.15	−4.41
33.3	−0.01	−0.22
42.9	2.53	2.15
55.6	2.67	2.52
63.6	2.84	2.73

illustrates the robustness of the simpler sc-NEVPT2 scheme. As for CASPT2, the relative energies of the MMCT state strongly depend on the nature of the reference wave function. Unphysical, negative transitions energies are obtained for reference wave functions optimized with a low weight on the MMCT state, while the ΔE tends to converge to more reasonable values in the case that the SA-CASSCF is biased to the MMCT state.

Due to the larger size of the CuMo model, we encountered some technical limitations in the code that prevented us to use the same SA-CASSCF reference wave function as in the CASPT2 calculations. Instead, we relied on the NEVPT2 implementation in ORCA (see Sect. 5.1), which allows us to treat larger systems. Unfortunately, we were not able to converge the CASSCF wave function increasing the weight on the MMCT state beyond 42.9 %. As shown in Table 3, the standard strongly contracted implementation of NEVPT2 is severely influenced by the poor description of the MMCT state in the reference wave function with 20 % weight on the MMCT state, for which negative excitation energies are obtained. Results gradually improve (as before) for larger weights, and better relative energies can be expected for reference wave functions with MMCT weights larger than 42.9 %. This standard procedure uses one set of orbitals for all states and only computes the orbital energies for the denominators for each state. Alternatively, one can generate canonical orbitals from the average orbitals for each state individually, this is, actually the default for CASPT2 and was also used in the NEVPT2 calculations for CuNi. This procedure takes slightly longer than the standard ORCA implementation but largely improves the results. Less negative energies are obtained for the reference wave functions with low MMCT weights, and the 42 % wave function gives results that are in reasonable agreement with the final CASPT2 estimate.

As an alternative to obtaining better orbitals by increasing the weight of the MMCT state in the optimization of the reference wave function, we have investigated the possibility to improve the orbitals by performing one state-specific orbital optimization step before entering the NEVPT2 calculation. As mentioned above, the orbital

Table 3 Strongly contracted, strongly contracted with state-specific canonicalized orbitals and partially relaxed NEVPT2 relative energies (in eV) of the MMCT state in the CuMo dimer as function of weight of the MMCT state in the SA-CASSCF reference wave function

% MMCT	sc-NEVPT2	sc-NEVPT2(ss)	pr-NEVPT2
20.0	−4.40	−2.32	0.62
33.3	−2.28	−0.01	1.93
42.9	−0.48	2.68	2.50

gradient of the different states is not zero at convergence of the SA-CASSCF. We have used this orbital gradient to make one step in the orbital optimization process of the MMCT state. A true single-state description is of course obtained when this path is followed until the gradient is zero, but this is actually not possible. Complete convergence on the orbitals cannot be obtained. This one-step orbital optimization does, however, significantly improve the behavior of the relative energy of the MMCT state. Now, we obtain positive excitation energies for all the reference wave functions. For the larger weights, the excitation energies are again comparable to the CASPT2 results. The one-step orbital optimization based on the reference wave function with 42.9 % MMCT weight gives a transition energy of 2.5 eV, which is in rather good agreement with the CASPT2 results, especially if one keeps in mind that further increase in the MMCT weight in the reference weight would lead to slightly higher relative energies.

In both models (CuNi and CuMo), the NEVPT2 energies behave rather similarly as we observed before for the CASPT2 calculations. The description of the MMCT state is deficient when standard SA-CASSCF procedures are followed to optimize the orbitals and more reliable transition energies are obtained when the weight of the MMCT state is increased in the orbital optimization process.

4 Time-dependent DFT

In this last section, we assess the possibilities to calculate the transition energy of the MMCT state in the CuMo model with time-dependent DFT. Based on the conclusions of previous investigations of the performance of TD-DFT for related transition metal compounds [98], we have made a selection of functionals from some of the different classes established by Perdew and collaborators [99]. From the local and gradient corrected functionals, we have taken the LDA, BP86 [100, 101], PBE [102], and OPBE [102–104] approximations. The B3LYP [105] and PBE0 [106, 107] have been taken as examples from the hybrid functionals, and we have selected two meta-GGAs: M06-2X [108] and TPSSh [99]. In addition, we also test the performance of

Table 4 Density functional relative energies (in eV) of the Mo/Cu(*d*–*d*) transitions and the MMCT state for different functionals

Functional	Cu(*d*–*d*)	Mo(*d*–*d*)	MMCT
PBE	1.42/1.54	2.32	1.58
	2.35/2.46	2.52	
OPBE	1.33/1.43	2.48	1.48
	2.27/2.27		
PBE0	1.48/1.49	2.31	3.64
	2.16/2.16	2.76	
B3LYP	1.51/1.52	2.28	3.08
	2.23/2.24	2.69	
M06-2X	0.84	2.18	
	1.26/1.26	2.63	
TPSSh	1.61/1.63	2.29	2.34
	2.49/2.57	2.67	
CAM-B3LYP	1.45/1.45	2.26	4.74
	2.16/2.16	2.78	

the CAM-B3LYP functional [109] in representation of the so-called range-separated functionals [110–112].

The LDA and BP86 functionals lead to rather delocalized orbitals that make the characterization of the excited states extremely difficult. For example, among the first fifty roots in the calculation with the BP86 functional, we have not been able to clearly identify the MMCT state using the basis sets of triple-zeta quality. Instead, with the basis set of split valence quality, the orbitals have a somewhat higher degree of localization and the MMCT state appears at 2.0 eV, while the lowest *d*–*d* transitions of Cu and Mo arise around 1.4 and 2.0 eV, respectively. The most relevant results obtained with the other functionals are summarized in Table 4.

The six different flavors show a remarkable coincidence as far as the Cu/Mo(*d*–*d*) transitions are concerned. Except M06-2X, all functionals show the same pattern of two pairs of nearly degenerate transitions around 1.4 ± 0.2 eV and 2.3 ± 0.2 eV for Cu and two distinct transitions around 2.3 eV and 2.7 eV for Mo. These values are in reasonable agreement with the CASPT2 estimates for the Mo(*d*–*d*) transitions (2.5/3.0 eV) given in Ref. [32] and the NEVPT2 values (2.6/3.3 eV). The TD-DFT results for the Cu(*d*–*d*) transitions are slightly higher than the 1.2 and 1.9 eV calculated with CASPT2.

The situation is different for the MMCT state. The scattering of the results is much larger, approximately 3 eV. The smallest transition energies of $\sim$1.5 eV are obtained with the gradient corrected PBE and OPBE functionals, while the long-range corrected CAM-B3LYP functional lies on the other extreme and predicts a transition energy of 4.7 eV for the MMCT state. The B3LYP result is in very good agreement with our final CASPT2 estimate and also favorably compares to the NEVPT2 estimate discussed in the previous section. Using the M06-2X functional, we have not been able to identify the Mo→Cu charge-transfer state among the first 45 roots ($\Delta E \leq$ 5.88 eV).

Only very recently, a new development in the range-separated functionals made possible an improved description of charge-transfer states in donor–acceptor complexes [113, 114]. The method involves a tuning of the range separation parameter such that the HOMO Kohn-Sham orbital energy is the opposite of the ionization potential. This procedure is capable of reproducing with high precision optical and fundamental gaps and also describes very well charge-transfer excitation energies at the absorption edge. The application of this method to the present model could possibly improve the behavior of standard TD-DFT and give more reliable energies, although the method needs to be tested for transition metal systems with open-shell electronic configurations in the ground state and has to prove its efficiency for states that are not at the absorption edge as is the case for the MMCT state in CuMo.

5 Conclusions

The standard description of MMCT states in binuclear TM complexes with multiconfigurational wave functions can give rise to serious artifacts and unrealistic negative excitation energies with respect to the ground state. The origin of this problem lies basically in the state-average orbital optimization procedure, which produces orbitals that are strongly biased toward the electronic configuration of the ground state. In general, other roots arising from the ground state electronic configuration (typically on-site *d*–*d* transitions) have lower CASSCF energies than the MMCT state and have to be included in the state average, making the weight of the MMCT state too small to ensure molecular orbitals sufficiently adapted to the charge-transfer state.

By gradually increasing the weight of the MMCT state in the state-average procedure, we smoothly approach the single-state description of this state and significantly improve the optimized orbitals to describe the charge-transfer state. The orbital gradient of this state is drastically reduced, and the subsequent MR-PT2 treatment of dynamic electron correlation behaves much better for larger MMCT weights in the reference wave function. Although the complete single-state description cannot be reached due to root flipping problems, the two cases that we have studied in this paper give stable results when the MMCT state has a weight of approximately 60 % in the state-average CASSCF orbital optimization. Exploratory calculations on the charge transfer in $LaMnO_3$ points to the same

conclusion; the ab initio description of the MMCT state requires to go beyond the standard SA-CASSCF procedure and one should carefully check the convergence of the resulting MR-PT2 excitation energy against variations of the weight of the MMCT state.

The study clearly indicates the key role of the molecular orbitals in the MR-PT2 description of the MMCT excitations. In order to situate this result in a more general frame, it is worth noticing that similar considerations have been recently reported in other contexts, namely the calculation of the vertical excitation energy of the $\pi \rightarrow \pi^*$ ionic excited states of organic molecules (in particular the *V* state of ethylene [115]) and of the magnetic coupling constant in binuclear Cu complexes [116]. In these studies, as in the present one, the difficulties found for a correct description of a given property have been related to the nature of the starting MOs. In particular, the orbitals obtained following a "*standard*" optimization procedure have shown to be strongly inadequate and to lead to unrealistic results. A close inspection on the nature of the wave function on which the optimization procedure is based has allowed to identify the origin of the problem and to propose appropriate strategies to overcome it. In all cases, the MR-PT2 approaches based on the proper set of orbitals give improved results, more in line with the experimental knowledge or with more refined theoretical methods.

It is encouraging to note that the two implementations of MR-PT2 that we have used here (CASPT2 and NEVPT2) give qualitatively the same results. Among the applied functionals, we can see that local density and gradient corrected functionals give reasonable estimates for the on-site *d–d* transitions, while they tend to underestimate the MMCT energies. The results for the other functionals are more difficult to classify. B3LYP seems to do a good job, PBE0 and TPSSh are also reasonable, but we have not been able to locate the MMCT state for the M06-2X functional. TD-DFT is obviously easier than the laborious procedure that we have outlined above (a series of CASSCF calculation varying the weight on the MMCT, and checking the dependence of the relative energy with the applied level shift in the CASPT2 part of the calculation), but the price to pay is that there seems to be no obvious best choice for the functional.

5.1 Computational information

CASPT2 calculations have been performed with MOLCAS 7.4 [117]; NEVPT2 calculations on the CuNi model with a program package developed at the University of Ferrara and interfaced to MOLCAS; and NEVPT2 calculations on the CuMo model have been done with ORCA 2.9 [118]. The sc-NEVPT2(ss) and pr-NEVPT2 variants listed in Table 3 were activated by adding the options "*nev_canonstep 1*" and "*nev_canonstep 3*" to the casscf block of the input. In all calculations for the CuNi model, the molecular orbitals are expanded in so-called atomic natural orbitals with (6*s*, 5*p*, 4*d*, 2*f*, 1*g*) basis functions for Cu and Ni, and (4*s*, 3*p*, 2*d*, 1*f*) functions for O [119, 120]. Slightly smaller basis sets of the same type have been used in the CASPT2 calculations for the CuMo dimer: Mo (7*s*, 6*p*, 5*d*, 2*f*), Cu (6*s*, 5*p*, 4*d*, 2*f*), the C and N atoms in the first coordination sphere of the metals (4*s*, 3*p*, 1*d*) and the other atoms a valence double zeta basis; (3*s*, 2*p*) for C and N, and (2*s*) for H. For the NEVPT2 calculations on the CuMo model, we used the *def2*-type of basis sets of the Ahlrichs group with triple-zeta + polarization for the metals [121] and the atoms in the first coordination sphere of these (8*s*, 6*p*, 5*d*, 2*f*, 1*g* (Mo); 6*s*, 5*p*, 4*d*, 2*f*, 1*g* (Cu); 5*s*, 3*p*, 1*d* (C,N)) and split valence + polarization for all the other atoms (3*s*, 2*p*, 1*d* (C,N); 2*s*, 1*p* (H)) [122]. To reduce the computation cost in the CuMo dimer, we have applied the Cholesky decomposition for CASPT2 [123, 124] and the Resolution of the Identity approximation for NEVPT2 [125]. TD-DFT calculations were performed with ORCA for all functionals, except OPBE, M06-2X, and CAM-B3LYP, for which the GAUSSIAN09 package [126] was used. The cartesian coordinates of the atoms in the two models can be found in the Supporting Information.

Acknowledgments Financial support has been provided by the Spanish Administration (Project CTQ2011-23140), the Generalitat de Catalunya (Project 2009SGR462 and Xarxa d'R+D+I en Química Teòrica i Computacional, XRQTC), and the European Union (COST Action CODECS CM1002).

References

1. Hartree DR, Hartree W (1936) Proc R Soc Lond Ser A 157:490
2. Worsley BH (1958) Proc R Soc Lond Ser A 247:390
3. Roothaan CCJ (1951) Rev Mod Phys 23:69
4. Watson RE (1960) Phys Rev 118:1036
5. Richardson JW, Nieuwpoort WC, RR Powell, Edgell WF (1962) J Chem Phys 36:1057
6. Nieuwpoort WC (1965) Philips Res Rep 6:1
7. Dahl JP, Ballhausen CJ (1968) In: Löwdin P-O (eds) Advances in quantum chemistry, vol 4. Academic Press, London, pp 170–226
8. Gagliardi L (2006) Theor Chem Acc 116:307
9. Richardson JW, Vaught DM, Soules TF, Powell RR (1969) J Chem Phys 50:3633
10. Gladney HM, Veillard A (1969) Phys Rev 180:385
11. Wachters AJH, Nieuwpoort WC (1972) Phys Rev B 5:4291
12. Wachters AJH, Nieuwpoort WC (1972) In: Clementi E (eds) Selected topics in molecular physics. Verlag-Chemie, Weinheim, p 135
13. Venkataramani S, Jana U, Dommaschk M, Sönnichsen FD, Tuczek F, Herges R (2011) Science 331:445
14. McGarvey JJ, Lawthers I (1982) J Chem Soc Chem Commun 906–907
15. Decurtins S, Gütlich P, Köhler CP, Spiering H, Hauser A (1984) Chem Phys Lett 105:1

16. Hauser A (2004) In: Gütlich P, Goodwin HA (eds) Spin crossover in transition metal compounds II. Springer, Berlin, vol 234 of series Top Curr Chem, pp 155–198
17. Brady C, McGarvey JJ, McCusker JK, Toftlund H, Hendrickson DN (2004) In: Gütlich P, Goodwin HA (eds) Spin crossover in transition metal compounds III. Springer, Berlin, vol 235 of series Top Curr Chem, pp 1–22
18. Ordejón B, de Graaf C, Sousa C (2008) J Am Chem Soc 130:13961
19. Cannizzo A, Milne CJ, Consani C, Gawelda W, Bressler C, van Mourik F, Chergui M (2010) Coord Chem Rev 254:2677
20. Gawelda W, Cannizzo A, Pham V-T, van Mourik F, Bressler C, Chergui M (2007) J Am Chem Soc 129:8199
21. Jeftic J, Hauser A (1997) J Phys Chem B 101:10262
22. Létard J-F, Real JA, Moliner N, Gaspar AB, Capes L, Cador O, Kahn O (1999) J Am Chem Soc 121:10630
23. Zein S, Borshch SA (2005) J Am Chem Soc 127:16197
24. Létard J-F, Carbonera C, Real JA, Kawata S, Kaizaki S (2009) Chem Eur J 15:4146
25. Sato O, Iyoda T, Fujishima A, Hashimoto K (1996) Science 272:704
26. Sato O, Einaga Y, Fujishima A, Hashimoto K (1999) Inorg Chem 38:4405
27. Sato O (2003) Acc Chem Res 36:692
28. Bleuzen A, Lomenech C, Escax V, Villain F, Varret F, Moulin C, Verdaguer M (2000) J Am Chem Soc 122:6648
29. Herrera JM, Marvaud V, Verdaguer M, Marrot J, Kalisz M, Mathonière C (2004) Angew Chem Int Ed 43:5468
30. Arrio A, Long J, Cartier dit Moulin C, Bachschmidt A, Marvaud V, Rogalev A, Mathonière C, Wilhelm F, Sainctavit P (2010) J Phys Chem C 114:593
31. Carvajal MA, Reguero M, de Graaf C (2010) Chem Commun 46:5737
32. Carvajal MA, Caballol R, de Graaf C (2011) Dalton Trans 40:7295
33. Bleuzen A, Marvaud V, Mathonière C, Sieklucka B, Verdaguer M (2009) Inorg Chem 48:3453
34. Coronado E, Dunbar K (2009) Inorg Chem 48:3293
35. Balzani V, Bergamini G, Campagna S, Puntotiero F (2007) In: Balzani V, Campagna S (eds) Photochemistry and photophysics of coordination compounds I. Springer, Berlin, vol 280 of series Top Curr Chem, pp 1–36
36. Otsuki J, Imai A, Sato K, Li D-M, Hosoda M, Owa M, Akasaka T, Yoshikawa I, Araki K, Suenobu T et al (2008) Chem Eur J 14:2709
37. Chen Y-J, Odongo OS, McNamara PG, Szacilowski KT, Endicott JF (2008) Inorg Chem 47:10921
38. Kim MW, Murugavel P, Parashar S, Lee JS, Now TW (2004) New J Phys 6:156
39. Anderson PW (1959) Phys Rev 115:2
40. Nesbet RK (1960) Phys Rev 119:658
41. Kahn O (1993) Molecular magnetism. VCH Publishers, New York
42. Van den Heuvel W, Chibotaru L (2007) Phys Rev B 76:104424
43. Calzado CJ, Angeli C, Taratiel D, Caballol R, Malrieu J-P (2009) J Chem Phys 131:044327
44. Calzado CJ, Angeli C, de Graaf C, Caballol R (2011) Theor Chem Acc 128:505
45. Tozer DJ, Amos RD, Handy NC, Roos BO, Serrano-Andrés L (1999) Mol Phys 97:859
46. Parac M, Grimme S (2002) J Phys Chem A 106:6844
47. Dreuw JL, Weisman A, Head-Gordon M (2003) J Chem Phys 119:2943
48. González L, Escudero D, Serrano-Andrés L (2011) ChemPhysChem 13:28
49. Barandiarán Z, Seijo L (1988) J Chem Phys 89:5739
50. Seijo L, Barandiarán Z (1999) In: Computational chemistry: reviews of current trends, vol 4. World Scientific, Singapore, p 55
51. de Graaf C, Hozoi L, Broer R (2004) J Chem Phys 120:961
52. Bordas E, de Graaf C, Caballol R, Calzado CJ (2006) Theor Chem Acc 116:535
53. Hay PJ, Wadt WR (1985) J Chem Phys 82:270
54. Winter NW, Pitzer RM, Temple DK (1987) J Chem Phys 86:3549
55. Zhang Y-Q, Luo C-L (2011) J Phys Chem A 115:7778
56. Roos BO (1999) Acc Chem Res 32:137
57. Serrano-Andrés L, Merchán M (2005) J Mol Struct (Theochem) 729:99
58. Vallet V, Macak P, Wahlgren U, Grenthe I (2006) Theor Chem Acc 115:145
59. Schreiber M, Silva-Junior MR, Sauer SPA, Thiel W (2008) J Chem Phys 128:134110
60. Sauri V, Serrano-Andrés L, Moughal Shahi AR, Gagliardi L, Vancoillie S, Pierloot K (2011) J Chem Theory Comput 7:153
61. Pierloot K (2011) Int J Quantum Chem 111:3291
62. Cabrero J, Caballol R, Malrieu J-P (2001) Mol Phys 100:919
63. Neese F (2003) J Chem Phys 119:9428
64. Barbatti M, Ruckenbauer M, Szymczak JJ, Aquino AJA, Lischka H (2008) Phys Chem Chem Phys 10:482
65. Hozoi L, Siurakshina L, Fulde P, van den Brink J (2011) Nature Sci Rep 1:65
66. Andersson K, Malmqvist P-Å, Roos BO, Sadlej AJ, Wolinski K (1990) J Phys Chem 94:5483
67. Andersson K, Malmqvist P-Å, Roos BO (1992) J Chem Phys 96:1218
68. Gagliardi L, Roos BO (2005) Nature 433:848
69. Blancafort L, Migani A (2007) J Am Chem Soc 129:14540
70. Huber SM, Moughal Shahi AR, Aquilante F, Cramer CJ, Gagliardi L (2009) J Chem Theory Comput 5:2967
71. Radon M, Broclawik E, Pierloot K (2011) J Chem Theory Comput 7:898
72. Giussani A, Merchán M, Roca-Sanjuán D, Lindh R (2011) J Chem Theory Comput 7:4088
73. Domingo A, Rodríguez-Fortea A, de Graaf C (2012) J Chem Theory Comput 8:235
74. Roos BO, Andersson K (1995) Chem Phys Lett 245:215
75. Forsberg N, Malmqvist P-Å (1997) Chem Phys Lett 274:196
76. Angeli C, Cimiraglia R, Malrieu J-P (2001) Chem Phys Lett 350:297
77. Angeli C, Cimiraglia R, Evangelisti S, Leininger T, Malrieu J-P (2001) J Chem Phys 114:10252
78. Angeli C, Cimiraglia R, Malrieu J-P (2002) J Chem Phys 117:9138
79. Andersson K, Roos BO (1992) Chem Phys Lett 191:507
80. Sousa C, de Jong WA, Broer R, Nieuwpoort WC (1997) Mol Phys 92:677
81. Pierloot K, De Kerpel JOA, Ryde U, Olsson MHM, Roos BO (1998) J Am Chem Soc 120:13156
82. González L, Daniel C (2006) J Comput Chem 27:1781
83. Coates R, Coreno M, DeSimone M, Green JC, Kaltsoyannis N, Kerridge A, Narband N, Sella A (2009) Dalton Trans 5943–5953
84. de Graaf C, Sousa C (2010) Chem Eur J 16:4550
85. Evangelio E, Bonnet M-L, Cabañas M, Nakano M, Sutter J-P, Dei A, Robert V, Ruiz-Molina D (2010) Chem Eur J 16:6666
86. Nakatani N, Hitomi Y, Sakaki S (2011) J Phys Chem B 115:4781
87. Liao P, Carter EA (2011) J Phys Chem C 115:20795
88. Pascual JL, Barandiarán Z, Seijo L (2011) Theor Chem Acc 129:545

89. Bokarev SI, Bokareva OS, Kühn O (2012) J Chem Phys 136:214305
90. Roos BO, Andersson K, Fülscher MP, Serrano-Andrés L, Pierloot K, Merchán M, Molina V (1996) J Mol Struct (TheoChem) 388:257
91. Radon M, Broclawik E (2007) J Chem Theory Comput 3:728
92. Chen H, Song J, Lai W, Wu W, Shaik S (2010) J Chem Theory Comput 6:940
93. Fujimori A, Minami F (1984) Phys Rev B 30:957
94. Broer R, Nieuwpoort WC (1981) Chem Phys 54:291
95. Malmqvist P-Å, Roos BO (1989) Chem Phys Lett 155:189
96. Queralt N, Taratiel D, de Graaf C, Caballol R, Cimiraglia R, Angeli C (2008) J Comput Chem 29:994
97. Angeli C, Cimiraglia R, Cestari M (2009) Theor Chem Acc 123:287
98. Escudero D, González L (2012) J Chem Theory Comput 8:203
99. Tao J, Perdew JP, Staroverov VN, Scuseria GE (2003) Phys Rev Lett 91:146401
100. Becke AD (1986) J Chem Phys 84:4525
101. Perdew JP (1986) Phys Rev B 33:8800
102. Perdew JP, Burke K, Ernzerhof M (1996) Phys Rev Lett 77:3865
103. Handy NC, Cohen AJ (2001) Mol Phys 99:403
104. Swart M, Ehlers AW, Lammertsma K (2004) Mol Phys 102:2467
105. Becke AD (1993) J Chem Phys 98:5648
106. Perdew JP, Ernzerhof M, Burke K (1996) J Chem Phys 105:9982
107. Adamo C, Barone V (1999) J Chem Phys 110:6158
108. Zhao Y, Truhlar DG (2008) Acc Chem Res 41:157
109. Yanai T, TDP, Handy NC (2004) Chem Phys Lett 393:51
110. Leininger T, Stoll H, Werner H-J, Savin A (1997) Chem Phys Lett 275:151
111. Tawada Y, Tsuneda T, Yanagisawa S, Yanai T, Hirao K (2004) J Chem Phys 120:8425
112. Jiménez-Hoyos CA, Janesko BG, Scuseria GE (2008) Phys Chem Chem Phys 10:6621
113. Stein T, Kronik L, Baer R (2009) J Am Chem Soc 131:2818
114. Kronik L, Stein T, Refaely-Abramson S, Baer R (2012) J Chem Theory Comput 8:1515
115. Angeli C (2009) J Comput Chem 30:1319
116. Angeli C, Calzado CJ (2012) J Chem Phys 137:034104
117. Aquilante F, De Vico L, Ferré N, Ghigo G, Malmqvist P-Å, Neogrady P, Pedersen TB, Pitoňák M, Reiher M, Roos BO et al (2010) J Comput Chem 31:224
118. Neese F (2012) ORCA—an ab initio, density functional and semiempirical program package, Version 2.9. Max Planck Institute for Bioinorganic Chemistry, Mülheim
119. Roos BO, Lindh R, Malmqvist P-Å, Veryazov V, Widmark P-O (2004) J Phys Chem A 108:2851
120. Roos BO, Lindh R, Malmqvist P-Å, Veryazov V, Widmark P-O (2005) J Phys Chem A 109:6575
121. Weigend F, Ahlrichs R (2005) Phys Chem Chem Phys 7:3297
122. Schäfer A, Horn H, Ahlrichs R (1992) J Chem Phys 97:2571
123. Koch H, Sánchez de Merás A, Pedersen TB (2003) J Chem Phys 118:9481
124. Aquilante F, Malmqvist P-Å, Pedersen TB, Ghosh A, Roos BO (2008) J Chem Theory Comput 4:694
125. Neese F (2003) J Comput Chem 24:1740
126. Frisch MJ, Trucks GW, Schlegel HB, Scuseria GE, Robb MA, Cheeseman JR, Scalmani G, Barone V, Mennucci B, Petersson GA et al (2009) Gaussian 09 revision A 0.2. Gaussian Inc., Wallingford